Fuel 105 (2013) 672–687

Contents lists available at SciVerse ScienceDirect

Fuel

journal homepage: www.elsevier.com/locate/fuel

Modeling the interface resistance in low soluble gaseous solvents-heavy oil systems

S. Reza Etminan [a,*], Mehran Pooladi-Darvish [a,b,1], Brij B. Maini [a,2], Zhangxin Chen [a,3]

[a] Chemical and Petroleum Engineering Department, University of Calgary, 2500 University Drive NW, Calgary, Alberta, Canada T2N 1N4
[b] Fekete Associates Inc., Calgary, Canada

HIGHLIGHTS

- Dilute dissolution of gases into heavy oil was modeled accounting for 3 parameters.
- The unknown parameters were diffusion and mass transfer coefficients and solubility.
- It models both equilibrium and non-equilibrium interface boundary conditions.
- This model uses the pressure decay data directly for the parameter estimation.
- Determination of k value does not necessarily imply for physical interface resistance.
- Correct modeling of interface physics leads to accurate estimation of the parameters.

ARTICLE INFO

Article history:
Received 11 July 2012
Received in revised form 23 August 2012
Accepted 28 August 2012
Available online 23 September 2012

Keywords:
Diffusion measurement
Solubility
Interface resistance
Pressure decay technique
Heavy oilBitumen

ABSTRACT

Measurement of gas diffusivity in reservoir fluids is of great interest for a number of applications, and among different methods for the measurement, the Pressure Decay method has received special attention due to its simplicity. In this technique, a non-volatile quiescent oil column is brought in contact with a diffusing single component gas from the top and the rate of change of gas pressure in the gas cap is recorded. The interpretation of outcomes is based on solution of a forward problem, which sometimes invokes a complicated boundary condition. In this work, an analytical solution is presented for the most general form of the boundary condition which models the interface. It takes into account all mass transfer key parameters including gas solubility, a diffusion coefficient and a possible interfacial resistance. The effect of resistance against mass diffusion at the interface is usually neglected in modeling. Through this solution, the role of interface resistance is better explained and one can realize how the resistance exactly affects the diffusion process. A detailed sensitivity analysis of each parameter is conducted and specifically in the case of interface resistance, it is illustrated that a numerical value can be reported for the interfacial resistance while it does not affect or hinder the diffusion process physically. This could unnecessarily increase the degree of freedom of the backward problem, and may lead to misleading parameter estimation results (despite a good match of the measurements). Using our new interface boundary condition reveals that some of the previous works on the modeling of interface resistance are subject to underestimation of the rate of gas dissolution which may lead to erroneous estimation of parameters.

1. Introduction

Transport phenomena involve the evolution of a system property in response to a non-equilibrium distribution of that property. In order for a system property to be transported, a spatial distribution of the property must exist and be different from that at equilibrium. Molecular diffusion is one of these transport phenomena playing a key role in petroleum engineering and is considered as a predominant mass transfer mechanism in many reservoir applications. Based on Fick's law, a diffusive flux is related to the concentration field, by postulating that the flux is proportional to the concentration gradient.

Accurate estimation of molecular diffusion is necessary for design and implementation of many of reservoir recovery scenarios. The rate of dissolution of injected gas in oil during secondary recovery [1], The rate of dissolution of injected carbon dioxide in brine during geological disposal of CO_2 [2,3], the rate of separation of gas from oil in solution gas drive mechanism [4] and the rate of injected gaseous solvents in bitumen during Vapour Extraction (VAPEX) [8–10,20] are all controlled by the molecular diffusion.

* Corresponding author. Tel.: +1 403 210 8730.
E-mail address: sretmina@ucalgary.ca (S. Reza Etminan).
[1] Tel.: +1 403 220 8779.
[2] Tel.: +1 403 220 8777.
[3] Tel.: +1 403 220 7825.

0016-2361/$ - see front matter © 2012 Elsevier Ltd. All rights reserved.
http://dx.doi.org/10.1016/j.fuel.2012.08.048

Nomenclature

A	diffusion cell cross sectional area (m^2)
C	mass concentration (kg/m^3)
D	diffusion coefficient (m^2/s)
H	Henry's law constant ($MPa/(kg/m^3)$)
h	height of bitumen column (m)
i	grid border index
J	sensitivity matrix
j	mass flux relative to mass-average velocity (kg/m^2 s)
k	film mass transfer coefficient (m/s)
M	group of coefficients
M_w	molecular weight (kg/kg – mole)
m	mass of gas dissolved (kg)
N	group of coefficients
n	mass flux relative to stationary velocity (kg/m^2 s)
P	pressure (MPa)
R	universal gas constant, 0.0083144 (MPa m^3/kg – mol K)
T	absolute temperature (K)
t	time (s)
V	volume (m^3)
w	gas mass fraction
Z	gas compressibility factor
z	vertical spatial coordinate (m)

Greek letters

ρ	density of mixture (kg/m^3)
λ	eigen-value
ρ	damping parameter
Ω	diagonal matrix
ε	integrated error

Superscripts

Asterisk	chemical equilibrium condition
n	time step coefficient
q	iteration number

Subscripts

b	bitumen
comp	computed
exp	experimental
eq	equilibrium
g	gas
gc	gas cap
i	initial condition
int	interface
m	mass
p	eigen values index

Abbreviations

Bw	between
BC	boundary condition
EOS	Equation of State
LHS	Left Hand Side
ODE	Ordinary Differential Equation
PR	Peng-Robinson
rms	root mean square
RHS	Right Hand Side
VAPEX	Vapour Extraction

There are a few experimental methods to estimate the magnitude of gas diffusion into a liquid. Among these different methods, those using a PVT cell in which two non-equilibrium phases are allowed to interact inside the cell at constant temperature are more attractive and powerful alternatives [5]. With proper description of the dissolution and evaporation process, diffusion coefficient can be inferred from changes in bulk properties such as a total mass, pressure and phase volume. Therefore, it is no longer necessary to intrude the model to take samples for compositional analysis and instead, the concentration change is determined from one of the above properties. This is an advantage of measuring the diffusion coefficient without direct measurement of the concentration change which is less cost effective and labor intensive. The approach in which a closed cell of fixed volume is used, the total mass of gas and liquid inside the PVT cell is constant, and the diffusion coefficient is inferred from the recorded changes in pressure and/or the liquid volume is known as the Pressure Decay [6] or Time-Resolved Pressure Detection [7] technique.

1.1. Pressure decay experiments and interface boundary conditions

The pressure decay experimental setup is a simple arrangement of a high precision transducer and a high pressure cell maintained at constant temperature. A column of oil is placed at the bottom of the diffusion cell and then gas fills the gas cap portion to a certain pressure. As the gas diffuses and dissolves into the heavy oil body, the gas cap pressure declines. This decay trend is continuously recorded versus time which acts as the main experimental measurements data in the pressure decay technique. A schematic of the pressure decay cell is shown in Fig. 1.

In 1996, Riazi [6] used methane and normal pentane in his pressure decay experiments. An equimolar counter-diffusion of these two species was modeled in which the initial concentration and location of gas–liquid interface were getting updated at the end of each time step. The interface concentration was obtained through calculation of average concentrations of each component and determination of the fugacities of components in each phase (using an Equation of State). The diffusion coefficient was constant during each time interval of Riazi's solution. The final numerical solution of his model provides changes of the average concentration and diffusion coefficient versus time. Zhang et al. [8] adapted Riazi's technique and introduced a simplified method which did not require recording of the interface position with time. Their

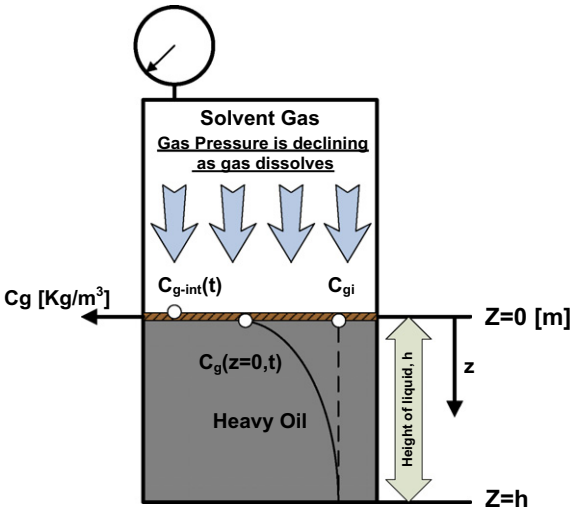

Fig. 1. Schematic of pressure decay cell and interface concentrations in presence of film resistance.

Table 1
Classification of Gas–Oil interface boundary conditions.

Authors	BC type @ interface	Boundary condition	Eq. no.
Zhang et al. (1999)	Dirichlet – constant	$C_g(z=0,t)=C_g^*(P_{eq})$	(1)
Upreti et al. (2000)	Dirichlet time dependent	$C_g(z=0,t)=C_g(t)$	(2)
Civan et al. (2001, 2002, 2006, 2009)	Robin – constant	$-D\frac{\partial C_g}{\partial z}\|_{z=0}=k(C_g^*(P_{eq})-C_g(z=0,t))$	(3)
Sheikha et al. (2005)	Neumann time dependent	$\frac{\partial C_g}{\partial z}\Big\|_{z=0}=M\frac{dC_g}{dt}$	(4)
Etminan et al. (2010)	Dirichlet – constant	$C_g(z=0,t)=C_g^*$	(5)
This work	Robin time dependent	$-D\frac{\partial C_g}{\partial z}\Big\|_{z=0}=k(C_{g\text{-}int}(t)-C_g(z=0,t))$	(6)

assumption of no change in the interface position is valid for the gas and oil systems where the oil volume change (swelling) is insignificant. Zhang et al. [8] used a Venezuelan oil sample and conducted their experiments with methane and carbon dioxide. They modeled this problem by assigning a saturation concentration at the interface, which in fact changes as system pressure reduces. But later in their analytical solution, a constant concentration at the interface, referred to as the equilibrium interface concentration, was considered as the boundary condition. This concentration was the equilibrium concentration when the pressure is not declining anymore (Eq. (1), Table 1). It caused the interface to act as a non-homogenous Dirichlet type boundary condition. This simplification and the real behavior of interface have been the issues of debate in the literature since then, and there has been no consensus on what boundary condition should be applied at the solvent-heavy oil interface.

By focusing more on solvent-heavy oil systems, *unidirectional* diffusion of gas into heavy oil has become central in modeling of these systems. Except Riazi's [6] original work and Haugen and Firoozabadi's [5] recent work , almost all other works have only modeled gas component dissolution into heavy oil. After Zhang et al. [8], Upreti et al. [9,10] conducted a series of experiments using methane, ethane, nitrogen, and carbon dioxide on two Canadian bitumen samples. They modeled the interface using a time-dependant Dirichlet boundary condition (Eq. (2), Table 1) and included swelling by using Mehrotra and Svrcek's [11] gas solubility and density data on the same oil. A variational numerical optimization technique, the conjugate gradient method with an adjoint problem for function estimation, was utilized in their work to estimate values of several parameters including the diffusion coefficient as a function of concentration.

Civan and Rasmussen [12–15] introduced a hindered mass transfer boundary condition. They assumed existence of a resistance to mass diffusion at the interface and as a result added a film mass transfer coefficient parameter to the modeling of this physics. This resistance is defined as the reciprocal of mass transfer coefficient parameter, k. Having two unknown mass transfer parameters, diffusion and mass transfer coefficients, introduces more difficulty into the solution of the forward and inverse problems. The interface boundary condition proposed by Civan and Rasmussen [12] is a third kind or Robin type boundary condition (Eq. (3), Table 1). The physics of film resistance is added into the boundary condition of the model while the diffusion partial differential equation remains the same. They used various experimental data from other authors [6–9] to estimate the values of unknown parameters.

Tharanivasan et al. [16] found this disagreement on the interface boundary condition interesting and worked on the comparison of the above three models. They called these three different boundary conditions as *equilibrium*, *quasi-equilibrium* and *non-equilibrium* boundary conditions, respectively, and concluded that depending on the type of dissolved gases, different boundary conditions should be applied for modeling of the interface. In 2006, they [17] extended their work by conducting three sets of experiments with a bitumen sample and methane, carbon dioxide and propane. Sheikha et al. [18] also introduced a new boundary condition that equated the rate of gas leaving the gas cap to the rate of gas diffusing into the oil body. It was a time-dependent Neumann (flux) type boundary condition assuming instantaneous equilibrium at the interface (Eq. (4), Table 1). They used Henry's law constant to relate the pressure of the gas cap to the interface gas concentration. They developed two graphical techniques to determine the value of diffusion coefficients for Upreti and Mehrotra's [9] experimental data. The value of Henry's constant was also calculated from Svrcek and Mehrotra's [11,19] gas solubility and density data for the Athabasca bitumen. Recently, Etminan et al. [20] introduced a modified pressure decay technique in which pressure was kept constant in the diffusion cell but pressure decline occurs in a supply cell which was connected to the diffusion cell gas cap. They used an equilibrium Dirichlet boundary condition which was constant in their experiment and was related to the gas cap pressure (Eq. (5), Table 1).

The objective of this work is to propose an improved version of the boundary condition when resistance exists at the interface. Scott et al. [21] stated that a situation where there is equilibrium (no resistance) at the interface is a special case of general treatment. Therefore, a general solution is sought which based on the values of k, is interchangeable between the solutions of equilibrium and non-equilibrium cases. Civan and Rasmussen [14] stated that if there is no resistivity at the interface of their proposed Robin type boundary condition (Eq. (3), Table 1), it is simplified the case of the Dirichlet boundary condition (Eq. (1), Table 1). This necessitates the interface concentration to be at saturation level at equilibrium case (no resistance). In this case, this solution inherits the difficulties which Zhang et al. [8] reported; i.e. having knowledge of equilibrium pressure is necessary. Besides that, in any measurement cases, if the pressure drop becomes large, even having a correct value of P_{eq} does not help. Because the concentration at the interface is not constant as the pressure in the gas cap reduces and its value is always larger than its equilibrium value. Our new boundary condition is a *time-dependent* Robin type boundary condition (Eq. (6), Table 1) and covers the whole range of equilibrium and non-equilibrium behaviors. Similar to Sheikha et al.'s [18] technique, declining gas cap pressure was related to the interface concentration (interface concentration at the gas side) through Henry's law constant which is correct for dilute solutions. An analytical solution is developed for this improved boundary condition which describes the physics of the interface more reasonably. This analytical solution is examined by Sheikha et al.'s [18] solution and a numerical approach. At the end, applicability of this model and its results are presented through estimation of mass transfer parameters using experimental data of other works [6,8,18].

The mathematical forms of the abovementioned boundary conditions for unidirectional gas diffusion into the oil body, including our proposed boundary condition are summarized in Table 1 as Eqs. (1)–(6). A detailed discussion of these equations will be given later in this article.

2. Statement of theory and mathematical model: forward problem

2.1. Diffusion model with interface resistance

Applying some reasonable assumptions for dissolution of low soluble gases into bitumen allows us to use Fick's second law as an appropriate diffusion model. Details of these simplifying assumptions and how the partial differential Eq. (7) is determined are presented in Appendix A.

$$\frac{\partial^2 C_g}{\partial z^2} = \frac{1}{D}\frac{\partial C_g}{\partial t} \tag{7}$$

Appropriate initial and boundary conditions, were applied to solve this problem. The initial condition of this problem is considered to be a bitumen sample which is devoid of gas.

$$C_g(z, t=0) = 0 \tag{8}$$

Based on Fig. 1, the boundaries are set at $z = 0$ and $z = h$. At $z = 0$, the boundary condition relates the rate of transfer of diffusing gas across the interface of the gas and bitumen system to the difference between the actual concentration at the interface at any time, $C_g(z = 0, t)$, and the concentration which is in equilibrium with the vapor pressure in the gas cap remote from the surface, $C_{g\text{-}int}(t)$. The discontinuity in concentrations across the interface is due to presence of a so-called film resistance which delays transfer of gas through two phases. This prevents instantaneous thermodynamic equilibrium at the interface and is modeled by a third kind (Robin type) boundary condition as follows:

$$-D\frac{\partial C_g}{\partial z}|_{z=0} = k(C_{g\text{-}int}(t) - C_g(z=0,t)) \tag{6}$$

This boundary condition is time-dependent since $C_{g\text{-}int}(t)$ is declining as pressure drops due to gas dissolution. k is the film mass transfer coefficient and $1/k$ is defined as the resistance. When an interfacial resistance is present against the gas molecular diffusion, a concentration discontinuity is formed across the interface; i.e. the instantaneous equilibrium concentration prevailing as a result of the bitumen interface contact with the gas cap ($C_{g\text{-}int}$), is not equal to the interface concentration ($C_g(z = 0, t)$) which is in continuum with the concentration profile in the oil phase. The concentration discontinuity at an interface is analogous to temperature discontinuity that is introduced at a gas–solid interface subject to cooling/heating. The two phases' interface is a monolayer of molecules, and therefore, mathematically no gas is accumulated at the interface and the interface volume is zero. For more lucidity, hereafter, $C_{g\text{-}int}$ is referred to as the "*concentration above the interface*" and $C_g(z = 0, t)$ is called the "*concentration below the interface*". A schematic of this difference in concentrations across the interface is shown in Fig. 1. The crosshatched surface on the top of heavy oil has exaggerated the interface thickness. The concentrations below the interface are part of a continuous concentration gradient but $C_{g\text{-}int}(t)$ is the instantaneous equilibrium concentration that would exist on both sides of the interface when there is no resistance. In this figure, a non-zero uniform initial concentration is considered.

Thermodynamically, Henry's law is valid when the dissolution amount of solute is small and the solution is dilute. In this range, the gas equilibrium pressure is related linearly to concentration [22]. The chemical equilibrium prevails instantaneously but only for concentration at the interface on the gas side of the interface (concentration above the interface). The equilibrium concentration $C_{g\text{-}int}(t)$ can be expressed by Henry's law, as in Eq. (9).

$$C_{g\text{-}int}(t) = \frac{P(t)}{H} \tag{9}$$

where H is Henry's law constant. The validity of using Henry's constant is elaborated in Appendix B.

Through a mathematical procedure, which is illustrated in Appendix C1, the boundary condition that is used for the solution of the diffusion equation is determined as Eq. (10).

$$\frac{\partial C_g}{\partial z}|_{z=0} = M\frac{dC_g}{dt}|_{z=0} - N\left[\frac{\partial^2 C_g}{\partial t \partial z}\right]_{z=0} \tag{10a}$$

In this boundary condition, M and N are defined as:

$$M = \frac{V_{gc}\cdot Mw\cdot H}{AZRTD} \tag{10b}$$

$$N = \frac{V_{gc}\cdot Mw\cdot H}{AZRTk} \tag{10c}$$

where V_{gc} is the volume of the gas cap, Mw is the gas molecular weight, A is the diffusion cell cross-sectional area, Z is the gas compressibility factor, R is the universal gas constant, and T is the absolute temperature. The boundary condition at the bottom of the cell ($z = h$) is considered to be of no-flow type as Eq. (11).

$$\frac{\partial C_g}{\partial z}|_{z=h} = 0 \tag{11}$$

The boundary value problem presented by Eqs. (6)–(9) are solved by using the Laplace transform method and its solution in the Laplace domain is as Eq. (12). Details of the solutions are shown in Appendix C2.

$$\overline{C}_g(z,s) = \frac{MP_i\left[\exp\left(\sqrt{\frac{s}{D}}(z-2h)\right) + \exp\left(-\sqrt{\frac{s}{D}}z\right)\right]}{H\left[\left(MS + (1+NS)\sqrt{\frac{s}{D}}\right) + \exp\left(-2\sqrt{\frac{s}{D}}h\right)\left(MS - (1+NS)\sqrt{\frac{s}{D}}\right)\right]} \tag{12}$$

In this equation, S denotes the variable of frequency domain; M and N are defined in Eqs. (10b) and (10c) and $\overline{C}_g$ is the gas concentration in the Laplace domain. An analytical closed-form of the Laplace inverse of Eq. (12) is not available; therefore, the Stehfest algorithm [23] is applied to find the inverse form numerically. In order to predict gas cap pressure using the proposed analytical method, the concentration values should be substituted from Eq. (12). If Eq. (6) is written using Henry's law constant to relate $C_{g\text{-}int}(t)$ to $P(t)$, then Eq. (13) is obtained.

$$P(t) = -\frac{DH}{k}\frac{\partial C_g}{\partial z}|_{z=0} + HC_g(z=0,t) \tag{13}$$

The calculated pressure is called P_{computed}, and then its value in the Laplace space is:

$$\overline{P}_{\text{computed}} = -\frac{DH}{k}\frac{\partial \overline{C}_g}{\partial z}|_{z=0,S} + H\overline{C}_g(z=0,S) \tag{14}$$

Differentiating Eq. (12) and substituting it into Eq. (14) leads to the value of P_{computed} in the Laplace domain as Eq. (15).

$$\overline{P}_{\text{computed}}(s) = \frac{MP_i\left(\left[\exp\left(-2h\sqrt{\frac{s}{D}}\right)+1\right] - \frac{D}{K}\left[\sqrt{\frac{s}{D}}\exp\left(-2h\sqrt{\frac{s}{D}}\right) - \sqrt{\frac{s}{D}}\right]\right)}{\left[\left(MS + (1+NS)\sqrt{\frac{s}{D}}\right) + \exp\left(-2\sqrt{\frac{s}{D}}h\right)\left(MS - (1+NS)\sqrt{\frac{s}{D}}\right)\right]} \tag{15}$$

where $\overline{P}_{\text{computed}}$ is the predicted gas cap pressure in the Laplace domain. The Laplace inverse of this value could be directly compared with experimental data. It is an advantage this method has because it eliminates all the calculations of the amount of gas dissolved values for the experiment and model to be compared with each other. The Laplace inverse of Eq. (15) allows us to find out how interface resistance could influence the pressure decay directly. Again, Stehfest algorithm [23] is required to find the inverse transform of Eq. (15).

Table 2
Specifications of pressure decay experiment used in our study.

Oil type: Bitumen from Syncrude in FortMcMurry, Alberta			
Solvent	CO_2	Initial pressure (MPa)	3.996
Bitumen height, h (m)	0.0101	Running time (h)	41.725
Gas cap height, h_{gc} (m)	0.0199	Cross sectional area of the cell (m^2)	7.854×10^{-3}
Initial solvent concentration (kg/m^3)	0	Bitumen volume in the cell (m^3)	7.932×10^{-5}
Temperature (°C)	75	Gas cap volume (m^3)	1.563×10^{-4}

3. Results and discussion

To demonstrate how our proposed forward solution in both regions of equilibrium and non-equilibrium conditions works at the interface and to compare it with other mathematical models, a set of representative parameters were employed. Upreti and Mehrotra [9] used CO_2 with the Athabasca bitumen in a pressure decay test at 75 °C. Data of this experiment was utilized by Sheikha et al. [18] and later by Rasmussen and Civan [15] to estimate the values of diffusivity and the mass transfer coefficient. The experiment's specifications and all the parameters estimated for this data set are presented in Tables 2 and 3, respectively. The reason for choosing this specific experiment was that it was the only experiment employed by three authors and its mass transfer parameters were estimated in these works and were available.

In Table 3, the empty spots are parameters which have not been reported. The parameters which have been used in this study are tabulated in the last column of Table 3, which hereafter is referred to as the *Base Case* parameters. The selection of the *Base Case* parameters, shown in Table 3, is also with due consideration of the parameters estimated in these Refs. [9,10,15,18]. The first three base case parameters are required for our proposed analytical solution and the last two are used to compare our model with Civan and Rasmussen's [12] solution.

3.1. Solution of the Base Case model

The boundary condition presented by Eq. (6) suggests that the discontinuity at the interface (shown by the right-hand-side, RHS) is proportional to the diffusive mass flux (shown by the left-hand-side, LHS). Therefore, it is expected that the largest value of discontinuity would appear at early time, when the flux has its biggest value. To compensate for the decline in the diffusive mass flux term on the LHS, the difference on the RHS should be diminishing. Regardless of how the concentration below the interface, $C_g(z=0,t)$, behaves, the concentrations above and below the interface approach each other and eventually reach the saturation concentration (C_g^*) which is obtained at the equilibrium pressure (P_{eq}).

Fig. 2 illustrates a profile of the gas concentration in the bitumen body after 12.225 h. Two concentrations exist at the interface:

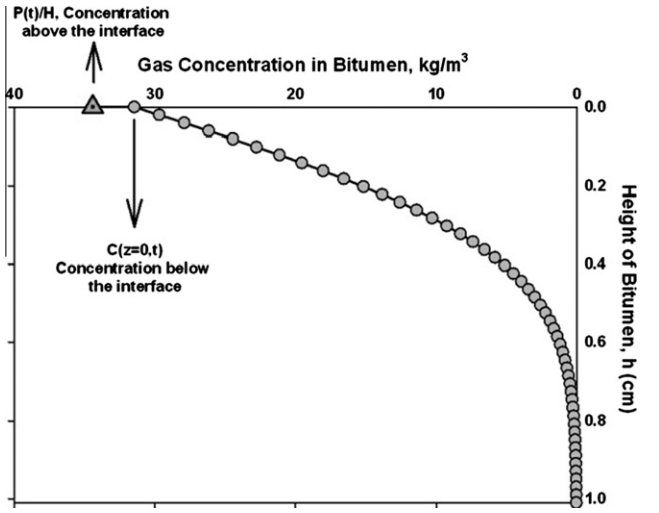

Fig. 2. Concentration profile in the bitumen column showing the interface concentrations at $t = 12.225$ h.

the triangular point at $z = 0$ showing the equilibrium concentration value of $P(t = 12.225\ h)/H$ and the first circular point at $z = 0$ displaying the $C_g(z = 0, t)$ term. The inequality of these two concentration values is because of the film resistance at the interface. This was schematically shown in Fig. 1. In the case of interface equilibrium when there is no resistivity, there would not be such difference and the concentration above and below the interface should be the same. To diffuse into the bitumen body, the gas molecules have to pass through the interface by overcoming this resistance and depending on the magnitude of the resistance; concentration below the interface might reach the equilibrium concentration either slower or faster.

The value of equilibrium pressure, P_{eq}, is provided by the solution of our model at a large value of time, beyond which, no more pressure decline occurs and the bitumen is fully saturated with diffusing gas at that temperature. The values of equilibrium pressure and saturation concentration for the Base Case are reported in Table 3. Fig. 3 depicts the concentration below and above the interface versus time, respectively. The equilibrium concentration above the interface, $C_{g\text{-}int}$, declines monotonically with time corresponding to the decreasing pressure. But the behavior of concentration below the interface, $C_g(z = 0, t)$ is different. At the early stages, the concentration below the interface increases but later when the difference between $C_g(z = 0, t)$ and $C_{g\text{-}int}$ has been diminished, it declines with time in concert with gas pressure decline. Physically, it means that initially the resistance at the interface dominates the transfer rate and whatever goes across the interface quickly diffuses into the bitumen body, which results in a low value of concentration at the interface. Later, as the concentration in

Table 3
Literature reported and Base Case parameters.

Parameters	Upreti et al. (2002) Method type	Sheikha et al. (2005)		Rasmussen et al. (2009)		Base Case
		Method 1	Method 2	Based on Sheikha et al.'s Method 1	Based on Sheikha et al.'s Method 2	
D (m^2/s)	3.74×10^{-10}	5.08×10^{-10}	4.64×10^{-10}	5.033×10^{-10}	4.894×10^{-10}	5.00×10^{-10}
k (m/s)				Infinity	1.426×10^{-6}	1.5×10^{-6}
H (MPa/(kg/m^3))		0.139[a]	0.139			0.11
P_{eq} (MPa)				3.13	3.13	3.15[b]
C^* (kg/m^3)				34.30	33.37	28.67[b]

[a] Extracted from Mehrotra et al. [11] data for Athabasca bitumen.
[b] These two values are calculated by running our model for a long time until reaching equilibrium pressure. Equilibrium concentration is determined from Henry's Law.

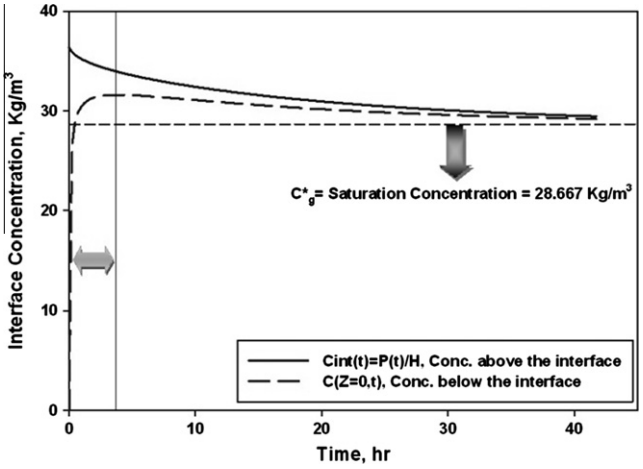

Fig. 3. Behavior of concentrations above and below the interface at $k = 1.5 \times 10^{-6}$ m/s.

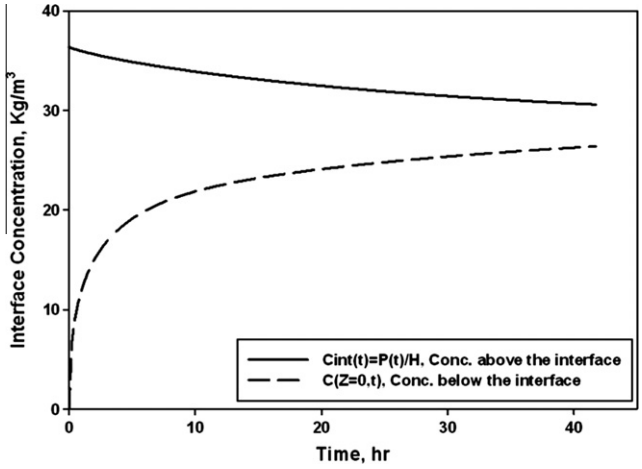

Fig. 5. Behavior of concentrations above and below the interface at $k = 1.5 \times 10^{-7}$ m/s.

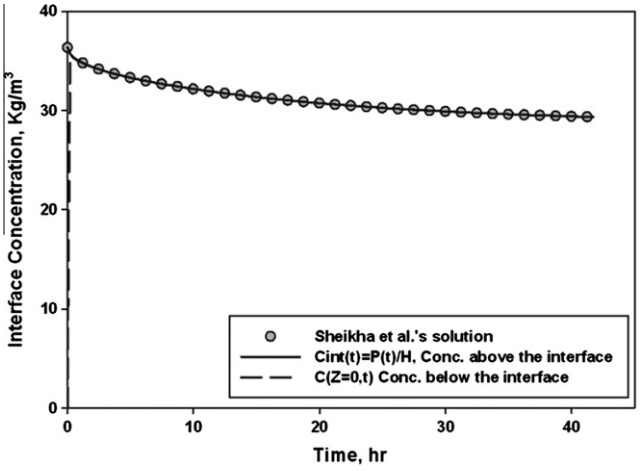

Fig. 4. Behavior of concentrations above and below the interface at $k = 1.5 \times 10^{-4}$ m/s – Comparison with Sheikha et al.'s solution.

the bitumen builds up, the diffusion in the liquid becomes the rate controlling mechanism and the influence of the interfacial resistance becomes less significant.

To better understand how the film resistance acts and controls the diffusion of gas into the bitumen, the Base Case is compared to two other cases, in one of which the resistance is 100 times smaller ($k = 1.5 \times 10^{-4}$ m/s, Fig. 4) and in the other with 10 times larger resistance ($k = 1.5 \times 10^{-7}$ m/s, Fig. 5). In Fig. 4, it is evident that the concentration below the interface has reached $C_{g\text{-}int}$ in a very short time and from there on, the two concentrations are declining together toward the saturation concentration. This situation is very similar to the equilibrium case presented by Sheikha et al.'s [18] boundary condition. Sheikha et al.'s [18] solution is also plotted in Fig. 4. From this comparison, it can be concluded that for particular values of mass transfer coefficients (here, larger than $k = 1.5 \times 10^{-4}$ m/s), the resistance at the interface can be neglected for all practical purposes and including mass transfer coefficient into the model does not necessarily and physically represent the interface resistance.

Fig. 5 illustrates the behavior of interface when the film resistance is 10 times larger. It can be seen that for larger film resistance, the concentration difference persists and the two concentrations will become equal only when the system is near equilibrium. It means that the resistance at the interface remains the controlling resistance much longer.

Fig. 6 displays how the magnitude of the mass transfer coefficient controls the flux of gas at the interface (Eq. (6)'s LHS). The $dC_g/dz|_{z=0}$ term is plotted on a logarithmic scale. The rate of the flux term decline at the interface is almost the same for the base case and the case with 100 times larger mass transfer coefficient but it is significantly lower for the case where film resistance is 10 times smaller. Fig. 7 shows the calculated gas cap pressure from Eq. (15) for the Base Case model and its approach toward the equilibrium pressure.

3.2. Model verification

Our proposed model was examined using two approaches: (1) by comparing with Sheikha et al.'s [18] solution when the resistance is negligible and (2) by evaluating its consistency with numerical solution of the same model. It is known that once there is equilibrium at the interface, the mass transfer coefficient goes to infinity (interface resistance goes to zero). Sheikha et al.'s [18] boundary condition is as Eq. (4) in Table 1. Using no flow boundary condition at the bottom of the diffusion cell, Sheikha et al.'s [18] solution becomes as Eq. (16):

$$\overline{C}_g(Z,S) = \frac{MP_i\left[\exp\left(\sqrt{\frac{S}{D}}(z-2h)\right) + \exp\left(-\sqrt{\frac{S}{D}}z\right)\right]}{H\left[\left(MS+\sqrt{\frac{S}{D}}\right) + \exp\left(-2\sqrt{\frac{S}{D}}h\right)\left(MS-\sqrt{\frac{S}{D}}\right)\right]} \tag{16}$$

A cursory look into our solution and Sheikha et al.'s [18] proves that Eqs. (12) and (16) are the same when k goes to infinity. In Eq. (12), as resistivity diminishes (k gets large values), N approaches zero and then this equation is identical to Eq. (16). Consistent with Scott et al.'s [21] statement that the equilibrium at the interface is a special case of general interface behavior, Sheikha et al.'s [18] solution is a special case of our general solution. Our solution is valid for a wider range of physical behavior.

In Sheikha et al.'s [18] solution, Henry's law is directly used as an auxiliary equation to relate interface equilibrium concentration to pressure; however, in our solution, Eq. (13) is applied.

When k is very large (no resistance), Eq. (13) becomes Eq. (9). The first term on the right hand side of Eq. (13) inserts a hindrance to the linear relation between the interface gas concentration and the gas cap pressure. This happens by subtracting a value from the first term on the RHS as long as equilibrium is not achieved. This delay in gas diffusion is related to the gradient of concentration

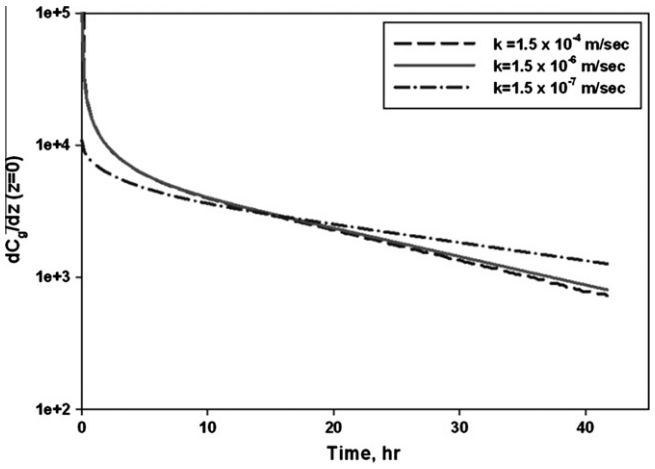

Fig. 6. Comparison of flux term at the interface for various k's.

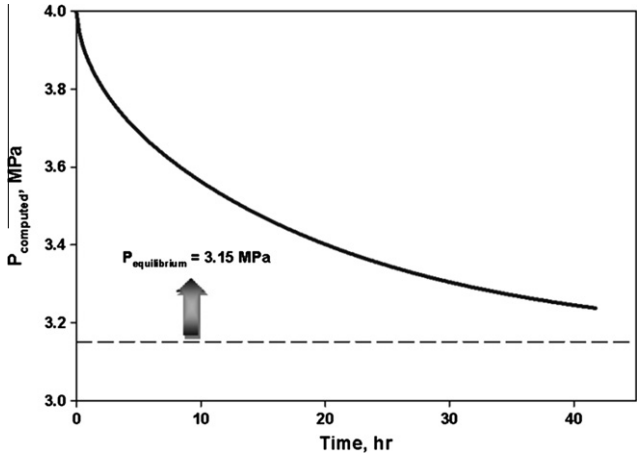

Fig. 7. Estimated pressure at the gas cap for the Base Case.

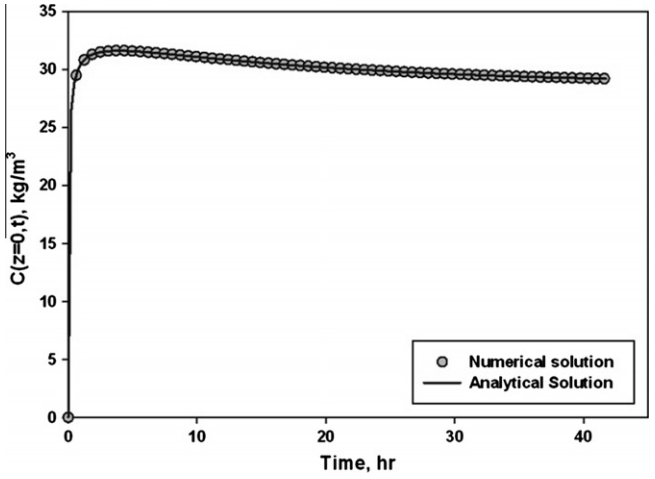

Fig. 8. Comparison of analytical and numerical solution for prediction of concentration below the interface.

at the interface and the values of mass transfer parameters. The concentration gradient is always decaying (as it was shown in Fig. 7) because the concentration of gas into the bitumen is rising as dissolution goes on. Fig. 4 demonstrates the agreement between

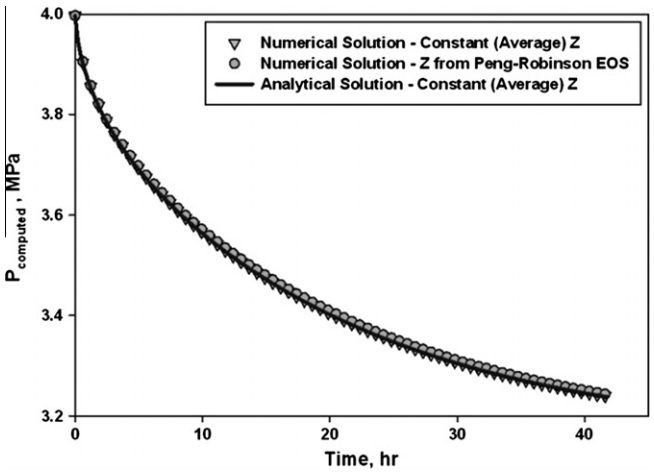

Fig. 9. Comparison of analytical and numerical solution for prediction of gas cap pressure – effect of using constant gas compressibility factor, Z versus Z from PR EOS.

Sheikha et al.'s [18] solution with our solution when the mass transfer coefficient is sufficiently large.

A one-dimensional numerical model was developed to examine the proposed analytical model and to check up the assumption of constant compressibility factor, Z. A fully implicit model was derived in which the unknown points were located on the border of the grids. This was beneficial in the sense that the discontinuity in the gas concentration has to be modeled at an interface with zero volume. The details of the numerical model are elaborated in Appendix D. The physical domain was discretized with 200 uniform grids and the time increment was 90 s.

Figs. 8 and 9 show the agreement between predicted $C_g(z = 0, t)$ and gas cap pressure for analytical and numerical solutions. This agreement between the two solutions reveals that the Stehfest Algorithm which was used to find the Laplace inverse transform of Eqs. (18) and (19) has almost no error. In Fig. 9, we also investigate the influence of using constant compressibility factor, Z, on our analytical solution and compare it with the numerical one in which the Peng-Robinson [24] Equation of State (EOS) was applied to predict the gas compressibility factor at the predicted pressures. The solid line in Fig. 9 shows the analytical gas prediction at an average compressibility factor equal to 0.881098 and it totally matches the numerical solution for the same constant value. The difference between the prediction of pressure using constant compressibility value and EOS is insignificant (See also Appendix E).

3.3. Sensitivity analysis on mass transfer parameters

A list of sensitivity cases evaluated is shown in Table 4. In this table, where values are not shown, the Base Case parameters are used. The effect of three parameters, including Henry's law constant (H), the diffusivity coefficient (D) and the film mass transfer coefficient (k), on the behavior of the analytical solution were investigated. The results studied are the concentration below the interface, the predicted gas cap pressure versus time for each case and the amount of gas dissolution versus time (determined from Eq. (19)).

3.3.1. Effect of Henry's Law constant (H)

Figs. 10.a and 10.b show the effect of Henry's law constant on the solution. The effect of Henry's constant variation is straightforward. If Henry's constant is defined as in Eq. (9), the equilibrium concentration at a given pressure is inversely proportional to H. It is consistent with the results produced in Fig. 10a. Once Henry's

Table 4
Sensitivity cases and values of each case.

Parameters	H (MPa/(kg/m^3))	D (m^2/s)	k (m/s)
Base Case	0.11	5.0×10^{-10}	1.5×10^{-6}
Effect of Henry's Law constant			
$H1$	0.07		
$H2$	0.09		
$H3$			
$H4$	0.13		
$H5$	0.15		
Effect of diffusion coefficient			
$D1$		5.0×10^{-12}	
$D2$		5.0×10^{-11}	
$D3$			
$D4$		5.0×10^{-9}	
$D5$		5.0×10^{-8}	
Effect of mass transfer coefficient			
$k1$			1.5×10^{-8}
$k2$			1.5×10^{-7}
$k3$			
$k4$			1.5×10^{-5}
$k5$			1.5×10^{-4}

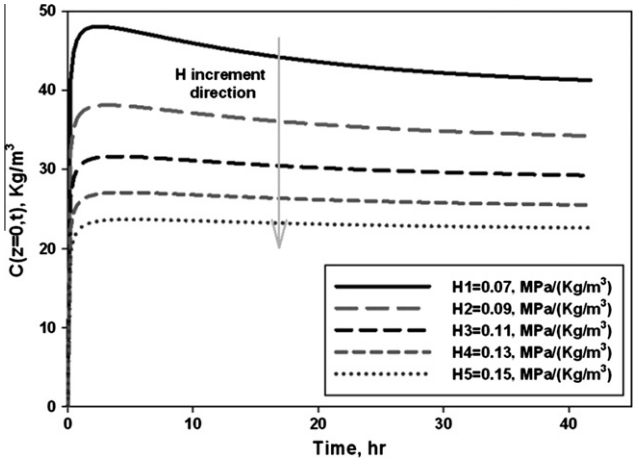

Fig. 10a. Effect of Henry's law constant on the concentration below the interface, $C_g(z = 0, t)$.

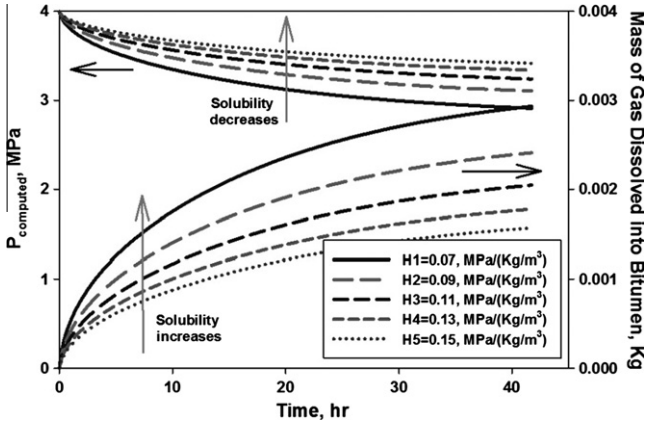

Fig. 10b. Effect of Henry's law constant on predicted gas cap pressure and the amount of gas dissolved.

constant is lower, the concentration at the interface stays higher. The results in Fig. 10b shows that as Henry's constant increases (solubility decreases), the gas pressure drops lesser (as the bitumen has a smaller capacity to absorb the gas). This figure also displays the amount of dissolution for different values of H which is consistent with the other two; so that for smaller values of Henry's constant, we have larger amount of gas dissolved into the bitumen. To summarize, for the same increment of Henry's constant, the concentration at the interface reduces less for higher H values; pressure also declines less before reaching the equilibrium pressure and gas dissolution is more as it goes toward smaller H's.

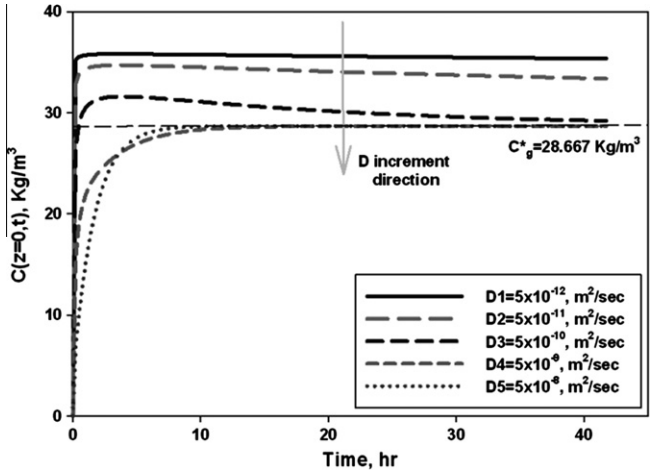

Fig. 11a. Effect of diffusivity coefficient on the concentration below the interface, $C_g(z = 0, t)$.

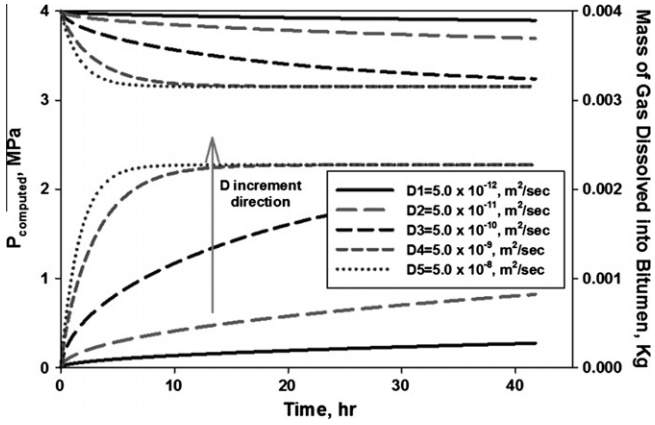

Fig. 11b. Effect of diffusivity coefficient on predicted gas cap pressure and the amount of gas dissolved.

3.3.2. Effect of diffusion coefficient (D)

The diffusion coefficient can be considered as the conductance resistance of bitumen body towards gas molecules' diffusion. As it was explained in Table 3, for the base case with Henry's constant of 0.11 MPa/(kg/m^3), the saturation concentration and equilibrium pressure are constant and equal to 28.667 kg/m^3 and 3.15 MPa, respectively. As time passes, all the graphs in Fig. 11a should approach the abovementioned saturation concentration and the curves in Fig. 11b should tend to the calculated equilibrium pressure and maximum dissolutions. When the diffusion coefficient is large, the gas diffuses into the bitumen very quickly and thus the concentration at the interface reaches the equilibrium concentration in a shorter time. In Fig. 11a, the curves for $D4$ and $D5$ have this characteristic. Therefore, as the concentration below the interface starts from zero, it reaches the saturation concentration rapidly without crossing the dashed line of saturation concentration.

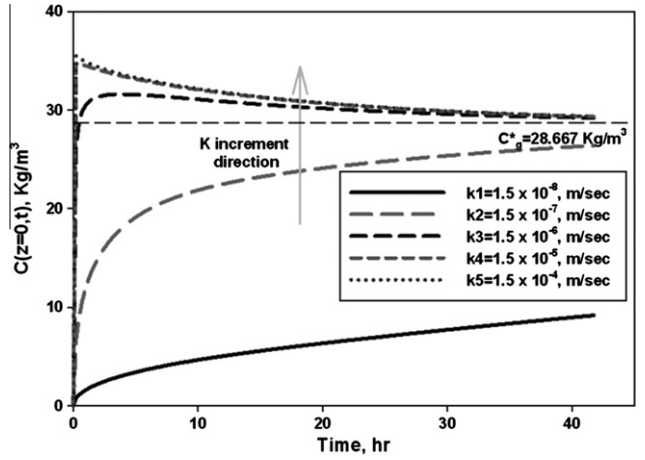

Fig. 12a. Effect of mass transfer coefficient on the concentration below the interface, $C_g(z = 0, t)$.

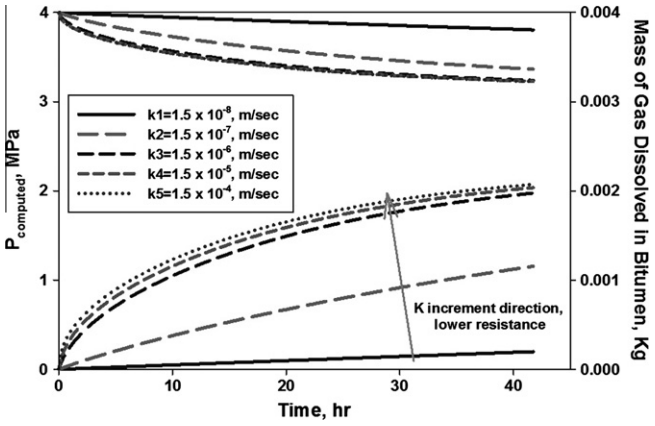

Fig. 12b. Effect of mass transfer coefficient on the predicted gas cap pressure and the mass of gas dissolved.

When the diffusion coefficient is very small ($D1$), it takes very long time for concentration to reach the saturation concentration because although gas can penetrate the interface (and below the interface concentration becomes larger than saturation concentration), it cannot easily diffuse into the bitumen body. The interplay between diffusion and mass transfer coefficients is also interesting. Fig. 11b shows the pressure prediction and demonstrates that when the gas diffuses easily into the bitumen body, it dissolves into the bitumen faster and therefore, gas cap pressure declines more rapidly. Fig. 11b also displays that for larger values of diffusion coefficients, amount of gas dissolution reaches its saturation plateau quite quickly whereas space-averaged gas dissolution amount is less for smaller diffusivity numbers in the same time frame.

3.3.3. Effect of mass transfer coefficient (k)

It was stated earlier that once the mass transfer coefficient becomes large, the resistance at the interface becomes insignificant. Depending on the ratio of mass transfer to the diffusion coefficient, the concentration at the interface might initially rise and approach the concentration above the interface and then decline with it towards the saturation concentration (cases of $k3$ to $k5$ in Fig. 12a) or it might gradually and monotonically move towards the saturation concentration (cases of $k1$ and $k2$ in Fig. 12a). Physically, when diffusion is dominant to interface resistance, as soon as gas molecules penetrate the interface, they immediately diffuse into the bitumen body and thus, no concentration build up occurs at the interface. However, when the resistance is significant, the concentration below the interface, $C_g(z = 0, t)$ goes even higher than saturation concentration (higher values like $C_g = P_{ini}/H$) and approaches the concentration above the interface and then from there, they decline together toward the saturation concentration. Fig. 12b illustrates that for smaller mass transfer coefficients (like $k1$), gas cap pressure reaches the equilibrium pressure over a longer time. It is apparent from this figure that for larger values of mass transfer coefficients, all pressure predictions lie on one line, which is the pressure decay line for the equilibrium interface (no resistance). The significance of each of these parameters needs a dimensionless analysis. Fig. 12b also shows that the amount of gas dissolution in a specific time for the cases of $k4$ and $k5$ is still different despite being very close to the equilibrium case. This means that $k4$ is still a physical resistance although very small. A very big difference is observed in the amount of gas dissolution and also pressure drop (both on Fig. 12b) between the orders of magnitude of 10^{-6} and 10^{-7} which means around these numbers the resistance at the interface becomes dominant in the dissolution process.

3.4. Comparison with an earlier analytical solution

Civan and Rasmussen [12–15] have investigated the effect of interface resistance for gas and liquid systems. Their proposed boundary condition for the gas–liquid interface is given by Eq. (3). They [12] presented the solution of the diffusion problem with this boundary condition as:

$$C_g = C_g^*\left[1 - 4\sum_{p=1}^{\infty}\frac{\sin(\lambda_p h)}{2\lambda_p h + \sin(2\lambda_p h)}\cos(\lambda_p(h - z))\exp(-\lambda_p^2 Dt)\right] \tag{17}$$

in which λ_p is the pth eigen-value determined from the following equation. The Newton method was applied to determine the eigen-values for the Base Case parameters and the first 25 eigen-values are used in our calculations.

$$\lambda_p \tan(\lambda_p h) = \frac{k}{D} \tag{18}$$

Civan and Rasmussen's [12] analytical model utilized the saturation concentration, C_g^* as the fixed concentration above the interface and as a result of this assumption, the concentration below the interface, $C_g(z = 0, t)$ is always capped to C_g^*. As we shown, this is not what happens all the time and is an approximation. Because the equilibrium concentration changes while the pressure drops and its minimum value is the saturation concentration. It means that for equilibrium concentrations larger than C_g^*, the RHS of Eq. (3) should be larger and therefore the flux on the LHS. Since the driving force for mass transfer across the interface is underestimated, the estimated k/D term should be larger (resistance or D should be smaller) to compensate for it. For a fixed resistance, their model would predict a smaller flux at the interface and consequently a lower rate of dissolution. This approximation could be severe if the difference between the initial and equilibrium pressure is large and the rate of pressure drop becomes slow. Fig. 13 demonstrates how simplification of assigning C_g^* as the above the interface concentration would affect $C_g(z = 0, t)$ behavior. This difference is such that the mass of gas dissolved is underestimated in their model for the same values of the resistance and diffusivity. The difference in the amount dissolved increases initially and then diminishes at large times. This implies that the underestimation is in the rate of gas dissolution which is led into determination of smaller diffusion coefficients.

The two curves in Fig. 13 are plotted for the Base Case parameters and as we showed, for mass transfer parameters close to

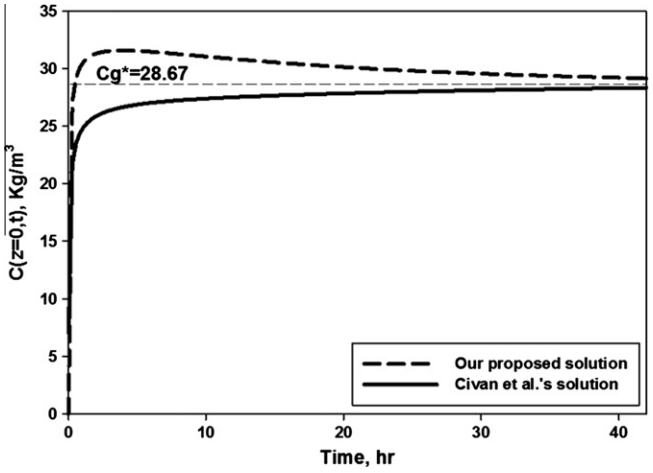

Fig. 13. Comparison between the predicted interface concentrations through our solution and Civan and Rasmussen's solution – Base Case parameters.

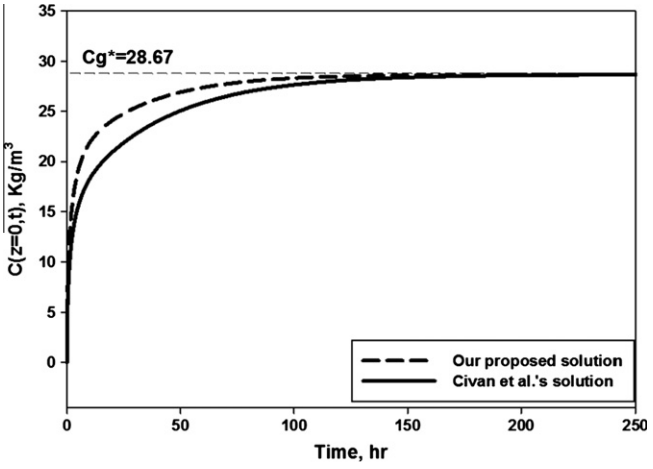

Fig. 15. Comparison between the predicted interface concentrations through our solution and Civan and Rasmussen's solution – Case of $k = 0.5 \times 10^{-7}$ m/s.

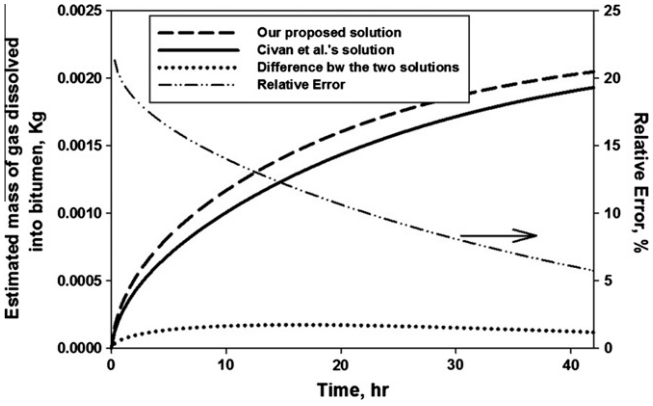

Fig. 14. Comparison between the predicted amounts of gas dissolved in bitumen through our solution and Civan and Rasmussen's solution – Base Case parameters.

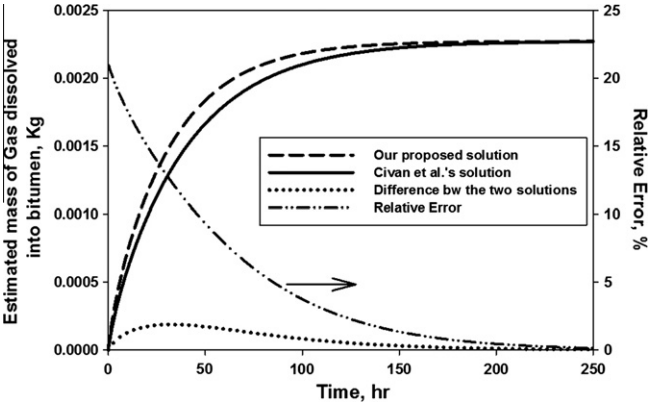

Fig. 16. Comparison between the predicted amounts of gas dissolved in bitumen through our solution and Civan and Rasmussen's solution – Case of $k = 0.5 \times 10^{-7}$ m/s.

Rasmussen and Civan's [15] parameters, the concentration below the interface exceeds the saturation concentration first and then declines to it asymptotically. However, Civan and Rasmussen's [12] solution for concentration gradually rises to the saturation value. When the amount of gas dissolution is determined from Eq. (19):

$$m_g(t) = \int_{z=0}^{z=h} C_g(z,t) A dz \tag{19}$$

then it can be shown that Civan and Rasmussen's solution underestimates the rate of gas dissolved in the bitumen body as shown in Fig. 14. Nevertheless, the amount of dissolutions for both cases reaches to the same value after about 200 h. Because Civan and Rasmussen's solution does not predict the gas cap pressure, the amount of gas dissolved is the only key value used for comparisons. The relative error graph reveals that the maximum discrepancy exists at the beginning and it diminishes toward the ultimate dissolution.

The difference between the two predictions in Fig. 14 was for the base case values in which Civan and Rasmussen's concentration profile was different from ours even in behavior (Fig. 13). Knowing that for smaller mass transfer coefficients (larger resistance) both interface concentrations would be monotonically increasing toward the saturation concentration, it was speculated that the concentration profile and rate of gas dissolution would be similar for both cases, but as it is shown in Figs. 15 and 16, the same discrepancy remains between the two solutions for the value of $k = 0.5 \times 10^{-7}$ m/s. Fig. 15 is plotted the concentrations for 250 h. It is evident the amount of dissolutions would be matched in a long run and only the rate of dissolutions are dissimilar which is exactly due to taking saturation concentration as the highest concentration at the interface. Fig. 16 shows that Civan and Rasmussen's boundary condition could lead to the underestimation of mass of gas dissolved of more than 5% for the first 100 h of this experiment.

4. Applications – inverse problem

An objective function was defined in a separate work of the same authors [25]. Using a modified form of the Gauss–Newton method, referred to as Levenberg–Marquardt algorithm [26–28], a code was generated which solves non-linear least square problems and obtains the values of three mass transfer unknowns: Henry's constant (H), diffusion coefficient (D) and mass transfer coefficient (k).

$$E(H,D,k) = \sum_{i=1}^{n} (P_{\exp}(t) - P_{\text{comp}}(t))^2 \tag{20}$$

In this equation, $P_{\exp}$ is the experimental measured pressure values vector, P_{comp} is the computed pressure based on our semi-analytical model, n is the number of measured pressure values and H, D, k are the unknown mass transfer parameters which are to be estimated

Table 5
Experiments' properties and estimated parameters.

Data Analysis	Riazi [6]	Zhang et al. [8]	Upreti et al. [9]	Tharanivasan et al. [17]
Known parameters				
Solute	CH_4	CO_2	CO_2	CO_2
Solvent	*n*-Pentane	Venezuelan oil	Bitumen	Bitumen
Temperature (°C)	37.8	21	75	23.9
Solvent height (m)	0.0768	0.07	0.0101	0.0435
Gas cap height (m)	0.21943	0.18	0.0199	0.1165
Cross sectional area (m^2)	5.15×10^{-4}	4.94×10^{-4}	78.54×10^{-4}	22.90×10^{-4}
Calculated parameters				
D (m^2/s) by experimenters	1.51×10^{-8}	4.8×10^{-9}	3.739×10^{-10}	9.4×10^{-10}[b]
k (m/s) by experimenters	–	–	–	1.128×10^{-7}[b]
D (m^2/s) (Tharanivasan et al. [16,17]) Equilibrium	–	4.1×10^{-9}	–	7.2×10^{-10}
D (m^2/s) (Tharanivasan et al. [16,17]) non-equilibrium	–	$>2.5 \times 10^{-8}$	–	5.7×10^{-10}
k (m/s) (Tharanivasan et al. [16,17])	–	$<2.143 \times 10^{-7}$	–	$>3.56 \times 10^{-7}$
D (m^2/s) (Civan and Rasmussen [14,15])	6.2×10^{-10}	1.13×10^{-8}	4.894×10^{-10}	–
k (m/s) (Civan and Rasmussen [14,15])	1.59×10^{-5}	3.26×10^{-7}	1.426×10^{-6}	–
P_{eq}/C_g[a] (MPa/(kg/m^3)) (Rasmussen and Civan [15])	–	–	0.0938	–
D (m^2/s) (Sheikha et al. [18]) Method 1	–	–	5.08×10^{-10}	–
D (m^2/s) (Sheikha et al. [18]) Method 2	–	–	4.64×10^{-10}	–
H (MPa/(kg/m^3))	–	–	~0.125[a]	0.0647[c]
D (m^2/s) our analysis	1.12×10^{-8}	6.202×10^{-8}	3.809×10^{-10}	3.558×10^{-10}
K (m/s) our analysis	9.2×10^{-6}	1.548×10^{-7}	3.808×10^{-7}	4.369×10^{-6}
H (MPa/(kg/m^3)) our analysis	0.1097	0.0855	0.10197	0.078735
Error (*rms*) our analysis with exp. data	0.044821	0.00906	0.002231	0.012503
Error (*rms*) Equilibrium (Sheikha) analysis with exp. data	0.0654112	0.21441	0.070290	0.012528
Integral Error - our analysis with exp. data	4.410×10^{-4}	1.393×10^{-3}	3.377×10^{-5}	9.856×10^{-4}
Integral Error Equilibrium (Sheikha) analysis with exp. data	1.844×10^{-3}	4.055×10^{-1}	4.112×10^{-2}	9.792×10^{-4}

[a] Not reported in the paper – calculated from [19].
[b] For short term data – diffusion time of 5 days.
[c] Calculated from Tharanivasan et al.'s paper [17].

through the inverse solution. The Levenberg–Marquardt (LM) method [26,27,29] is given by the following iterative form:

$$\begin{bmatrix} k \\ H \\ D \end{bmatrix}^{(q+1)} = \begin{bmatrix} k \\ H \\ D \end{bmatrix}^{(q)} + \left[(J^{(q)})^T J^{(q)} + \mu^{(q)} \Omega^{(q)} \right]^{-1} \times (J^{(q)})^T \left[\vec{P}_{\exp} \quad -\vec{P}_{\text{comp}} \left(\begin{bmatrix} k \\ H \\ D \end{bmatrix}^{(q)} \right) \right] \tag{21}$$

in which the superscript q is the iteration number and J is the sensitivity matrix calculated at the iteration q. In this equation, $\mu^{(q)}$ is a positive scalar named damping parameter and $\Omega^{(q)}$is a diagonal matrix defined as:

$$\Omega^{(q)} = \text{diag}\left[(J^{(q)})^T J^{(q)} \right] \tag{22}$$

The matrix term $\mu^{(q)}\Omega^{(q)}$ is used to damp the oscillations and instabilities due to the ill-conditioned character of such problems. Details of this method, its application and pitfalls are presented in authors' other work [25].

Using our code, we estimated the values of three sets of experimental data available in the literature. The experimental data belong to Riazi [6], Zhang et al. [8], Upreti and Mehrotra [9], and Tharanivasan et al. [17]. The first three sets have been used by Civan and Rasmussen [14,15] for estimation of the mass transfer parameter and diffusion coefficient which can be an appropriate source for comparison. The last set belongs to Tharanivasan et al.'s [17] work, in which they investigated all sorts of interface boundary conditions. The experiment from Upreti and Mehrotra's [9] work is the Base Case experiment we used earlier for all the sensitivity analysis in this paper.

Two sorts of errors are defined to address the difference between the predicted pressure based on the best estimated parameters and experimental pressures. The first one is a root-mean-square error shown in Eq. (23) and the second one is an integrated error as Eq. (24).

$$rms = \left[\frac{1}{N_t} \sum_{i=1}^{Nt} [P_{\exp}(t_i) - P_{\text{comp}}(t_i)]^2 \right]^{1/2} \tag{23}$$

$$\varepsilon = \frac{\int_0^t [P_{\exp}(t) - P_{\text{comp}}(t)]^2 dt}{\int_0^t [P_{\exp}(t)]^2 dt} \times 100\% \tag{24}$$

where N_t is the number of measurements.

Properties of each of these experiments and all the estimated values from different works and the corresponding errors are illustrated in Table 5.

The first experiment belongs to Riazi [6]. Methane and normal pentane are the solute and solvent used in this pioneering work. Riazi [6] has reported a diffusion coefficient to be equal to 1.51×10^{-8} m^2/s. The value our model estimated is 1.12×10^{-8} m^2/s which is very close to Riazi's prediction. The value Civan and Rasmussen's model predicted is about 100 times smaller. In terms of the resistivity measurement, our approach estimates the mass transfer coefficient to be equal to 9.2×10^{-6} m/s. Fig. 17 shows the quality of the matching between Riazi's experimental results, our model and Sheikha's model which is the equilibrium case (where there is no resistance) of our model. As it is evident, the errors are quite small and our model matches the whole range. On the other hand, the Sheikha et al.'s solution is very close to our solution for the same diffusion coefficient and Henry's constant. The errors reported at the bottom of Table 5 displays how close these two solutions are. This exactly denotes what was mentioned earlier; a numerical value could be reported for the mass transfer coefficient while it does not affect the problem physically. Here 9.2×10^{-6} m/s is a value reported for this mass transfer coefficient but as it was shown in Fig. 17, this experiment could be easily modeled without including for interface resistance which reduces degree of freedom of this backward solution.

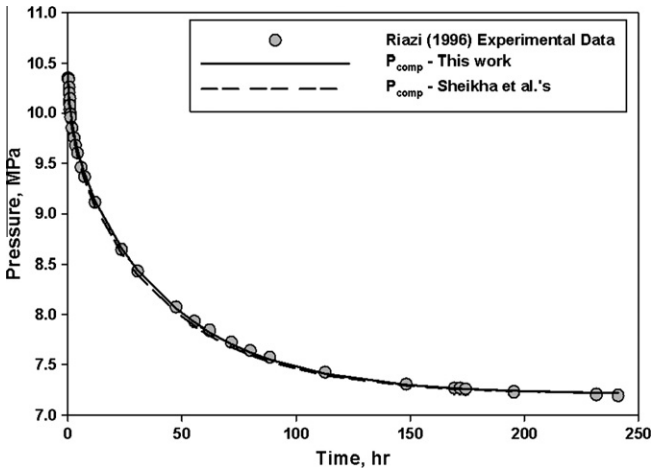

Fig. 17. History matching of calculated pressures using Riazi experimental data, this work's model and Sheikha et al.'s (equilibrium) model.

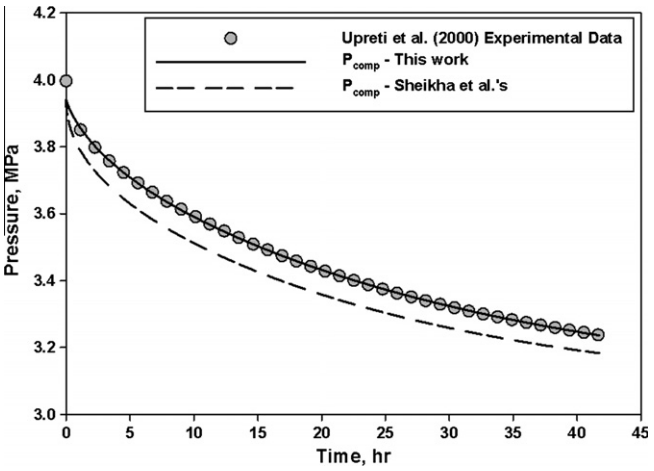

Fig. 19. History matching of calculated pressures using Upreti et al. experimental data, this work's model and Sheikha et al.'s (equilibrium) model.

The next experiment is Zhang et al.'s [8] work. They used an interface equilibrium boundary condition (Dirichlet's type) equal to saturation concentration. The estimated values of the diffusion coefficient using the equilibrium boundary condition is in the order of 10^{-9} for Zhang et al. [8] and Tharanivasan et al.'s [12,13] analysis of the same data. However, it is in the order of 10^{-8} for the cases with the inclusion of interface resistance. Tharanivasan et al. reported this value to be larger than 2.5×10^{-8} m^2/s and our estimated value is 6.202×10^{-8} m^2/s. Our estimated value is also in agreement with Tharanivasan's and is close to Civan and Rasmussen's estimated mass transfer coefficient. Fig. 18 shows how the predicted pressure (based on our model and estimated parameters) matches Zhang et al.'s experimental data. This figure shows how Sheikha et al.'s equilibrium model's predicted pressure is far away from experimental data using same D and H determined from our model. This implies that including the resistivity parameter is a must in this experiment. Once no resistivity is used and Sheikha et al.'s equilibrium case is using a diffusion coefficient of the order 10^{-8}, the diffusion has been 10 times faster and that is why Sheikha et al.'s [18] predicted pressure drops quite fast. However, resistance at the interface helps to have a better match. The reported errors show how equilibrium prediction is led to a mismatch.

Upreti et al.'s data for CO_2 dissolution in bitumen in 75 °C is the third set. Upreti and Mehrotra predicted a concentration dependent diffusion coefficient for this experiment using a quasi-equilibrium boundary condition which does not account for interface resistance. They reported $D = 3.739 \times 10^{-10}$ m^2/s as the diffusion coefficient average value. Our predicted diffusivity is very close to this value. Our predicted mass transfer coefficient is an order of magnitude smaller than Civan and Rasmussen's prediction which refers to a larger interface resistivity. Fig. 19 shows the agreement between the experimental data and our model's predicted pressure. The discrepancy between our model's and Sheikha et al.'s solutions shows that value of $k = 3.808 \times 10^{-7}$ m/s is a physical resistance at the interface and not just a number.

The last experiment belongs to Tharanivasan et al.'s [17] work in 2006. In their work, they estimated diffusion coefficients for different diffusion time ranges. The values with two asterisks in Table 5 belong to the diffusion and mass transfer coefficients of less than 5 days. The non-equilibrium case for the full range of diffusion time obtains the diffusion and mass transfer coefficients as 5.7×10^{-10} m^2/s and values larger than 3.56×10^{-7} m/s, respectively. This is in agreement with the value of the same parameters our model estimated. Unlike the two previous experiments, here the value of $k = 4.369 \times 10^{-6}$ m/s is almost like no resistance situation such that the predicted pressure from our model coincides with Sheikha et al.'s solution. Fig. 20 displays how the equilibrium and non-equilibrium cases match each other on the experimental data.

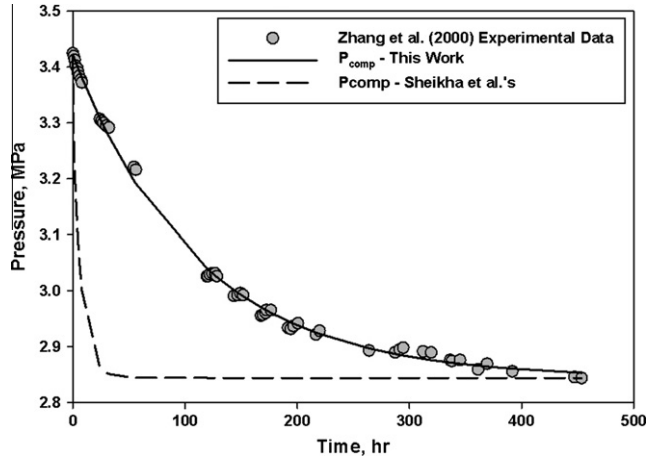

Fig. 18. History matching of calculated pressures using Zhang et al. experimental data, this work's model and Sheikha et al.'s (equilibrium) model.

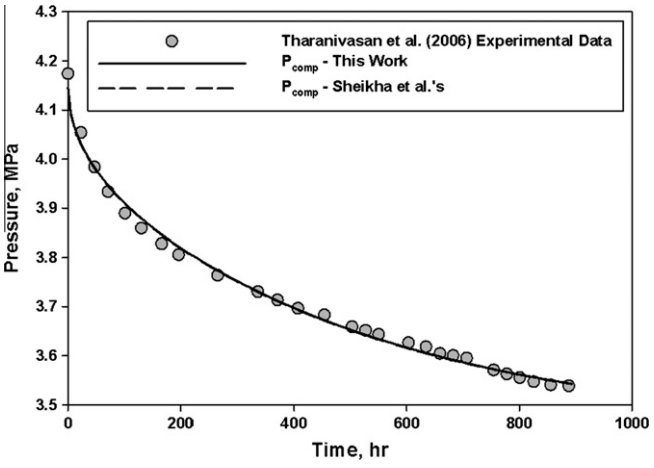

Fig. 20. History matching of calculated pressures using Tharanivasan et al. experimental data, this work's model and Sheikha et al.'s (equilibrium) model.

5. Conclusions

In this study, an improved analytical solution has been developed for the pressure decay experiment, which is able to model both the *equilibrium* and the *non-equilibrium* boundary conditions. This solution has been used to understand the role of film resistance at the gaseous solvents/bitumen interface. Unlike the other available solutions for modeling the resistance at the interface, this model accounts for the relationship between the gas cap pressure decline and the concentration at the interface. This allows for comparing the analytical solution directly with collected experimental data, which significantly lessens the volume of calculations for estimation of unknown parameters. This proposed method does not apply a constant equilibrium concentration at the interface for entire time of the experiment which could lead to underestimation of the amount of gas dissolution with respect to time. Through using this method, it is unraveled that determination of a large value for the mass transfer coefficient would indicate no physical interface resistance against mass transfer. Determination of an accurate forward model leads to improved interpretations of the pressure decay tests and more reliable estimation of the diffusion parameters.

Sensitivity analysis of three mass transfer parameters on our proposed boundary condition at the interface reveals that: (i) for lower Henry's constants, the solubility and saturation concentration is higher at the interface and the gas cap pressure drop is larger; (ii) the lower the diffusion coefficient, the longer it takes for the interface concentration to reach to the equilibrium; (iii) based on the magnitude of interface resistance, the concentration at the interface may exceed the saturation concentration and then reduces asymptotically toward it or it may never exceed the saturation concentration and just moves toward saturation.

Acknowledgments

The first author acknowledges the financial support by National Sciences and Engineering Research Council (NSERC), Canada. Also, generous funding by NSERC/AIRI (AIEES)/Foundation CMG/iCORE (AITF) chairs is highly appreciated.

Appendix A

General. diffusion model and Fick's Second Law

Many engineering applications involve the transfer of material across the interface between two phases. Eq. (7) has been used in many diffusion measurement publications recently but it is important to investigate the simplifying assumptions which allow us to use this equation.

A system of pure gas diffusion into the bitumen phase can be counted as a binary system, if the bitumen is considered as one component. In this case, Eqs. (A1), (A2), (A3) describe the diffusion model for this system [30].

$$n_{gz} = C_g u_g \tag{A1}$$

$$j_{gz} = C_g(u_g - u) \tag{A2}$$

$$u = \frac{1}{\rho}\sum_k C_k u_k = [w_g u_g + w_b u_b] \tag{A3}$$

In Eq. (A1), n_{gz} is the gas mass flux relative to a stationary coordinate, C_g is gas concentration and u_g is the mean velocity of gas components in the z direction with respect to stationary coordinate. In Eq. (A2), j_{gz} is the gas mass flux relative to the mass-average velocity and u id defined as in Eq. (A3). w_g and w_b are the gas and bitumen mass fractions respectively and are equal to C_k/ρ where ρ is the density of the mixture. In the case of gas diffusion into bitumen, the volatility of the system liquid is negligible and a unimolal unidirectional model will describe the system very well. In this case, n_{bz} is equal to zero.

If j_g is substituted by the diffusional flux, Eq. (A4) is determined.

$$j_{gz} = -\rho D\frac{dw_g}{dz} \tag{A4}$$

where z is the vertical coordinate and D is the molecular diffusion coefficient. In this equation, ρ is not necessarily constant and if we extend w_g, then:

$$j_{gz} = -D\left[1 - \frac{C_g}{\rho}\frac{\partial\rho}{\partial C_g}\right]\frac{\partial C_g}{\partial z} \tag{A5}$$

If we combine Eqs. (A2) and (A5), then the following equation is determined:

$$n_{gz} = -\frac{D}{1-w_g}\left[1 - \frac{C_g}{\rho}\frac{\partial\rho}{\delta C_g}\right]\frac{\partial C_g}{\partial z} + C_g u_b \tag{A6}$$

As it is evident, this flux contains a diffusive and also a convective term. Once mass conservation is applied using the above equation, then the non-linear differential Eq. (A7) is obtained.

$$\frac{\partial}{\partial z}\left[\frac{D}{1-w_g}\left[1 - \frac{C_g}{\rho}\frac{\partial\rho}{\partial C_g}\right]\frac{\partial C_g}{\delta z}\right] - \frac{\partial}{\partial z}(C_g u_b) = \frac{\partial C_g}{\partial t} \tag{A7}$$

Once no volume change happens in the bitumen due to gas dissolution, the bitumen mean velocity would be zero and the convective term in Eq. (A7) is crossed off the equation. In this case, the bitumen is motionless and the whole system could be derived based on a stationary coordinate (using n_{gz} rather than i_{gz}).

Using several reasonable assumptions allows us to simplify the above equation to Fick's second law and permit for an analytical solution.

The whole incorporated assumptions in this work are:

(1) Bitumen is motionless and swelling of bitumen due to gas dissolution is negligible (dilute solutions).
(2) Gas diffusion is unidirectional and bitumen is non-volatile ($n_{bz} = 0$).
(3) Solution density remains constant and does not change with concentration alteration (is correct only in dilute solutions).
(4) The diffusion coefficient is constant.
(5) There is no chemical reaction between the diffusing gaseous solvent and bitumen.
(6) Density gradient is positive in the direction of gravity; i.e., natural convection does not occur.
(7) The gas compressibility factor is assumed to be constant over the pressure range involved in the test.

Assumptions 1 and 2 are already applied to develop Eq. (A7). Using assumption 3 simplifies Eq. (A7) to the following equation:

$$\frac{\partial}{\partial z}\left(D\frac{\partial C_g}{\partial z}\right) = \frac{\partial c_g}{\partial t} \tag{A8}$$

Applying assumption 4 linearizes the above diffusion equation and leads to Fick's second law as Eq. (7) in the paper:

$$\frac{\partial^2 C_g}{\partial z^2} = \frac{1}{D}\frac{\partial C_g}{\partial t} \tag{7}$$

Assumption 7 allows us to solve the problem analytically. The study in Appendix E shows the order of the error that this assumption exerts on our work.

Appendix B

Application. of Henry's Law constant

Henry's law constant is valid for dissolution of sparingly soluble gases in bitumen. Tharanivasan et al.'s [17]measurement proves the linear relationship between the pressure change and concentration in experiments with CO_2, methane and propane. Our own experiments with many gases at different pressures and with different bitumen samples show similar behavior. Based on this experience, we can also state that neglecting volume change due to mixing (swelling) is a valid assumption only for sparingly soluble gases, i.e. gases that obey Henry's law. Therefore, the use of Henry's law is justified in systems where swelling is negligible. That is why we limited the application of our model to low-soluble gases specifically.

The low soluble gases we are referring to are methane, carbon dioxide and nitrogen. Based on the operating conditions (pressure and temperature) in which gas is injected and diffusing, there might be different amount of solubilities. For those ranges of solubilities which the vapor pressure of gas is linearly proportional to concentration through the Henry's law, our method is applicable. This could be valid for lower solubility ranges of high soluble gases like propane or butane as well which the deviation from linearity is not yet significant.

It is important to note that this limitation in using low soluble gases exists once concentration below the interface is coupled with gas cap pressure (through Eq. (13)). This is where Henry's law constant appears in equations. The behavior of concentration at the interface (Eq. (12)) and its difference with the concentrations determined from previous works (Eq. (17)) is independent of using Henry's law is applied to relate interface concentration to pressure.

Appendix C

C.1. Interface boundary condition derivation

If both sides of Eq. (6) are differentiated with respect to time and are rearranged, we get:

$$\frac{\partial C_{g\text{-}int}}{\partial t} = \frac{\partial C_g}{\partial t}\Big|_{z=0} - \frac{D}{k}\frac{\partial^2 C_g}{\partial t \partial z}\Big|_{z=0} \tag{C1.1}$$

In Eq. (C1.1), $C_{g\text{-}int}$ can be replaced by $C_g(z=0,t)$ to give a uniform equation based on the concentration below the interface. A material balance of gas dissolving into the bitumen is considered as follows. Regardless of the presence of resistance at the interface and because the interface has no volume, whatever gas leaves the gas cap diffuses into the bitumen. In other words, the rate of pressure reduction in the gas cap should be proportional to the rate of gas diffusion in the bitumen. Using a general Equation of State, the mass of gas leaving the gas cap is related to the gas cap pressure. Technically, Z is changing with pressure too but for simplicity and as it was addressed above, it is assumed to be constant over the range of pressures involved in the test in our solution. Eq. (C1.2) relates the rate of mass transfer from the gas cap to the pressure decline rate.

$$\frac{dm_g}{dt} = -\frac{V_{gc}Mw}{RTZ}\frac{dP}{dt} \tag{C1.2}$$

On the other hand, Fick's first law is used for finding the rate of gas dissolution into the bitumen body.

$$\frac{dm_{gD}}{dt} = -DA\frac{dC_g}{dz}\bigg|_{z=0} \tag{C1.3}$$

Equating Eqs. (C1.2) and (C1.3) provides a relation between $C_g(z=0,t)$ and the pressure drop.

$$\frac{dP}{dt} = \frac{RTZDA}{V_{gc}Mw}\frac{dC_g}{dz}\Big|_{z=0} \tag{C1.4}$$

Using Henry's law constant, Eq. (9), to relate the gas cap pressure into the instantaneous equilibrium concentration above the interface connects the two values of the concentration on both sides of the resistive interface as follows:

$$\frac{dC_{g\text{-}int}}{dt} = \frac{AZRTD}{H\cdot V_{gc}\cdot Mw}\frac{dC_g}{dz}\Big|_{z=0} \tag{C1.5}$$

Substituting Eq. (C1.5) into the left-hand side (LHS) of Eq. (C1.1), gives an equation in terms of $C_g(z=0,t)$. Eq. (10) is determined as the new form of our proposed boundary condition.

C.2. Forward solution of diffusion problem using laplace transform

Using the Laplace transform of diffusion the partial differential equation is given by Eqs. (C2.1).

$$\int_0^\infty \frac{d^2C_g}{dz^2}e^{-st}dt = \frac{d^2\overline{C}_g}{dz^2} = \frac{1}{D}[S.\overline{C}_g - I.C.] \Rightarrow \frac{d^2\overline{C}_g}{dz^2} - \frac{S}{D}\overline{C}_g = 0 \tag{C2.1}$$

Solving the above simple ODE gives:

$$\overline{C}_g(z,S) = A'\cdot\exp\left(\sqrt{\frac{S}{D}}z\right) + A''\cdot\exp\left(-\sqrt{\frac{S}{D}}z\right) \tag{C2.2}$$

where A' and A'' are two arbitrary constants. Using Eq. (11), A' and A'' are related to each other as Eq. (C2.3).

$$\frac{A'}{A''} = \exp\left(-2\sqrt{\frac{S}{D}}h\right) \tag{C2.3}$$

For the boundary condition at the interface, once we get the Laplace transform from both sides, and solve the right-hand side (RHS) of the Laplace transform integrals through the method of integration by part, Eq. (C2.4) is reached.

$$\frac{d\overline{C}_g}{dz}\Big|_{z=0} = M\left[-\frac{P_i}{H} + S.\overline{C}_g|_{z=0}\right] - N\left[-\frac{dC_g}{dz}\Big|_{z=0,t=0}\right] + S.\frac{c\overline{C_g}}{dz}\Big|_{z=0} \tag{C2.4}$$

In this ODE, $\partial C_g/\partial z|_{z=0,t=0}$ is zero. It means that at zero time, no gradient exists at the interface. If Eqs. (C2.2) and (C2.4) are used together, A'' is determined as follows:

$$A'' = \frac{MP_i}{H\left[\left(MS + (1+NS)\sqrt{\frac{S}{D}}\right) + \exp\left(-2\sqrt{\frac{S}{D}}h\right)\left(MS - (1+NS)\sqrt{\frac{S}{D}}\right)\right]} \tag{C2.5}$$

A' is calculated from (C2.3) and (C2.5) and finally the concentration in the Laplace domain is determined as Eq. (12).

Appendix D

Numerical. model description

Fig. D1. shows the schematic of the discretized heavy oil body. Diffusion Eq. (7) was discretized in the central scheme and a forward discretization was applied for the boundary conditions. All the grey points on the discretized body are unknown and by having i available equations, it is possible to find the unknown values. The discretized form of the diffusion equation and boundary conditions in locations $z(1)$, $z(2)$ and $z(i)$ are shown below.

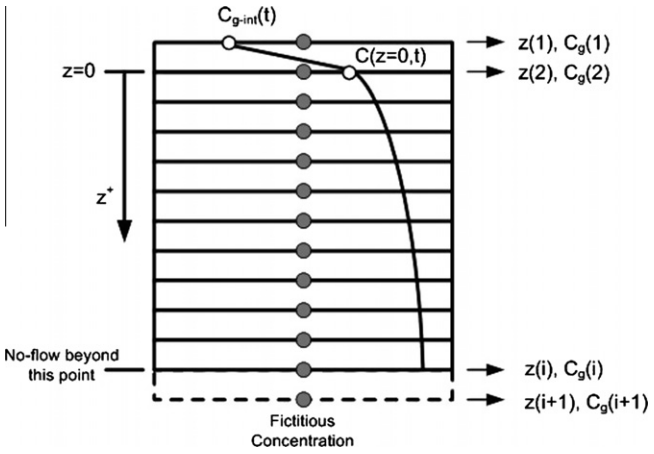

Fig. D1. Numerical model discretization.

$$\frac{C_g^{n+1}(i-1)-2C_g^{n+1}(i)+C_g^{n+1}(i+1)}{\Delta z^2}=\frac{1}{D}\frac{C_g^{n+1}(i)-C_g^{n}(i)}{\Delta t} \tag{D1}$$

No gas can be accumulated in the first grid and between borders $z(1)$ and $z(2)$. Thus the rate of gas entering $z(1)$ should be equal to the rate of gas leaving $z(2)$ to be dissolved into the oil body. Thus:

$$n_g(1)=-D\frac{dC_g}{dz}|_{z(1)}=-\frac{H\cdot V_{gc}\cdot Mw}{AZRT}\frac{dC_g(1)}{dt} \tag{D2}$$

$$n_g(2)=-D\frac{dC_g}{dz}|_{z(2)}=k(C_g(1)-C_g(2)) \tag{D3}$$

Equating these two equations leads to the ordinary differential Eq. (D4) which acts as an additional equation.

$$\frac{dC_g(1)}{dt}=\frac{1}{N}[C_g(2)-C_g(1)] \tag{D4}$$

where N is exactly the same N in Eq. (10c). The discretized form of the above equation is given as Eq. (D5).

$$\frac{C_g^{n+1}(1)-C_g^{n}(1)}{\Delta t}=\frac{1}{N}[C_g^{n+1}(2)-C_g^{n+1}(1)] \tag{D5}$$

As it is seen, no Δz is incorporated into Eq. (D5) and since this equation comes from a material balance over a zero-volume interface, this ODE is valid at any z and can also be valid at $z = 0$. It is evident that a value of $C_g(1)$ should be known at an earlier time at the beginning of the simulation run which at $t = 0$, $C_g(1) = P_i/H$.

$z(2) = 0$ acts as the main interface boundary point and thus Eq. (6) is valid at this point. The forward discretized form of the above-mentioned equation is as follows.

$$-D\frac{C_g^{n+1}(3)-C_g^{n+1}(2)}{\Delta z}=k(C_g^{n+1}(1)-C_g^{n+1}(2)) \tag{D6}$$

Finally, at the bottom of the cell, the diffusion flux is zero and thus we have:

$$\frac{C_g^{n+1}(i+1)-C_g^{n+1}(i)}{\Delta z}=0 \tag{D7}$$

The final fictitious grid's thickness is considered to be very small. Using all the equations leads to the matrix of coefficients which is tridiagonal for our one dimensional model. It is simply solved by the Thomas Algorithm, the best algorithm for a tridiagonal system Ozisik [31] and Chen [32].

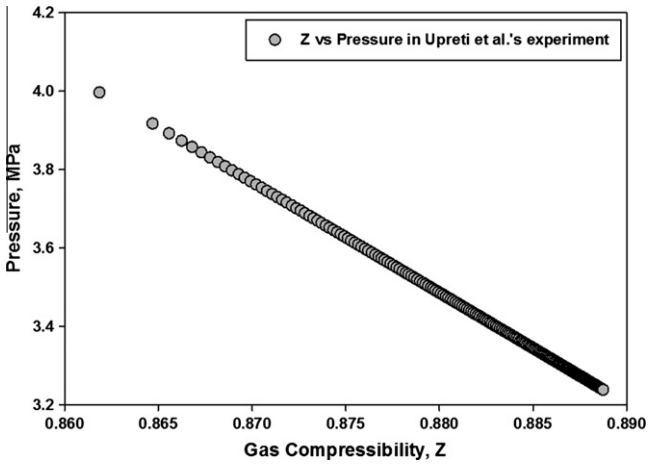

Fig. E1. Change of gas compressibility factor with pressure using Peng-Robinson EOS in Upreti et al.'s experiment for CO_2 and bitumen in 75 °C.

Table E1
Effect of using constant compressibility factor on estimated mass transfer parameters.

	Z_{min} (P_{ini})	Z_{max} ($P_{leaving}$)	Average Z[a]
K (m/s) × 10^7	3.8086	3.8086	3.8086
H (MPa/(kg/cm^3))	0.099777	0.10289	0.10197
D (m^2/s) × 10^{10}	3.8089	3.8089	3.8089

[a] Data used in Table 5.

Appendix E

Effect. of using constant gas compressibility factor

The gas compressibility factor used in our work is the average value of gas compressibility factors changing with decaying pressure and constant temperature in the range of pressure drop. The difference between using the average gas compressibility value and altering Z from the Peng-Robinson EOS is depicted on Fig. 9. In this section, the sensitivity of estimated mass transfer parameters to the constant values of the gas compressibility factor is studied.

Fig. E1. shows how the Z factor is changing with pressure in the range of pressure drop in Upreti et al.'s experiment. The maximum and minimum Z values in the leaving and initial pressures, respectively, were used in our analysis to calculate the mass transfer parameters in these two constant values. Table E1 tabulates the estimated values for mass transfer parameters in these two states. As it is obvious in this table, the values of mass transfer and diffusion coefficients do not change at all for different values of Z; however, Henry's constant value is changing a bit. This makes sense because the value of Z affects the amount of gas dissolution but not the rate of gas dissolution. Henry's constant variation is also not very significant. Nevertheless, taking Z as a constant is something which needs to be investigated for the cases in which we are applying it and we cannot generalize its correctness everywhere. In cases where the pressure drop is significant, it may or may not be an issue. However, in these cases, using a constant concentration at the interface is definitely an issue as Tharanivasan et al. [17] showed in their work.

References

[1] Renner T. Measurement and correlation of diffusion coefficients for CO_2 and rich-gas applications. SPE Reservoir Eng 1988;3(2):517–23.

[2] Farajzadeh R, Zitha PLJ, Bruining J. Enhanced mass transfer of CO_2 into water: experiment and modeling. Ind Eng Chem Res 2009;48(13):6423–31.
[3] Hassanzadeh H, Pooladi-Darvish M, Keith DW. Scaling behavior of convective mixing, with application to geological storage of CO_2. AIChE J 2007;53(5):1121–31.
[4] Shahvali M, Pooladi-Daarvish M. Dynamic modelling of solution-gas drive in heavy oils. J. Can. Pet. Technol. 2009;48(12):39–46.
[5] Haugen KB, Firoozabadi A. Mixing of two binary nonequilibrium phases in one dimension. AIChE J 2009;55(8):1930–6.
[6] Riazi MR. A new method for experimental measurement of diffusion coefficients in reservoir fluids. J Petrol Sci Eng 1996;14(3–4):235–50.
[7] Sachs W. The diffusional transport of methane in liquid water: method and result of experimental investigation at elevated pressure. J Petrol Sci Eng 1998;21(3–4):153–64.
[8] Zhang Y, Hyndman C, Maini B. Measurement of gas diffusivity in heavy oils. J Petrol Sci Eng 2000;25(1–2):37–47.
[9] Upreti SR, Mehrotra AK. Experimental measurement of gas diffusivity in bitumen: results for carbon dioxide. Ind Eng Chem Res 2000;39(4):1080–7.
[10] Upreti SR, Mehrotra AK. Diffusivity of CO_2, CH_4, C_2H_6 and N_2 in Athabasca bitumen. Can J Chem Eng 2002;80(1):116–25.
[11] Mehrotra AK, Svrcek WY. Correlations for properties of bitumen saturated with CO, CH, and N, and experiments with combustion gas mixture. J Can Petrol Tech 1982;21(6).
[12] Civan F, Rasmussen ML. Accurate measurement of gas diffusivity in oil and brine under reservoir conditions. Paper SPE; 2001. p. 67319.
[13] Civan F, Rasmussen ML. Improved measurement of gas diffusivity for miscible gas flooding under nonequilibrium vs. equilibrium conditions. Paper SPE; 2002. p. 75135.
[14] Civan F, Rasmussen M. Determination of gas diffusion and interface-mass transfer coefficients for quiescent reservoir liquids. SPE J 2006;11(1):71–9.
[15] Rasmussen ML, Civan F. Parameters of gas dissolution in liquids obtained by isothermal pressure decay. AIChE J 2009;55(1):9–23.
[16] Tharanivasan AK, Yang C, Gu Y. Comparison of three different interface mass transfer models used in the experimental measurement of solvent diffusivity in heavy oil. J Petrol Sci Eng 2004;44(3–4):269–82.
[17] Tharanivasan AK, Yang C, Gu Y. Measurements of molecular diffusion coefficients of carbon dioxide, methane, and propane in heavy oil under reservoir conditions. Energy Fuels 2006;20(6):2509–17.
[18] Sheikha H, Pooladi-Darvish M, Mehrotra AK. Development of graphical methods for estimating the diffusivity coefficient of gases in bitumen from pressure-decay data. Energy Fuels 2005;19(5):2041–9.
[19] Svrcek W, Mehrotra A. Gas solubility, viscosity and density measurements for Athabasca bitumen. J Can Petrol Technol 1982;21(4).
[20] Etminan SR, Maini BB, Chen Z, Hassanzadeh H. Constant-pressure technique for gas diffusivity and solubility measurements in heavy oil and bitumen. Energy Fuels 2010;24(1):533–49.
[21] Scott E, Tung L, Drickamer H. Diffusion through an interface. J Chem Phys 1951;19:1075.
[22] Olander DR. General thermodynamics. CRC; 2008.
[23] Stehfest H. Algorithm 368: numerical inversion of laplace transforms [D5]. Commun ACM 1970;13(1):47–9.
[24] Danesh A. PVT and phase behaviour of petroleum reservoir fluids, vol. 47. Elsevier Science; 1998.
[25] Etminan SR. Determination of mass transfer parameters in solvent based oil recovery techniques. Society of Petroleum Engineers, SPE International Student Paper Contest, Annual Technical Conference and Exhibition (ATCE2012), 8–10 October 2012, San Antonio, TX.
[26] Ozisik MN, Orlande HRB. Inverse heat transfer: fundamentals and applications. Taylor & Francis; 2000.
[27] Mittrapiyanuruk, P., A memo on how to use the levenberg-marquardt algorithm for refining camera calibration parameters. Website; 2006 <http://cobweb.ecn.purdue.edu/~kak/courses-i-teach/ECE661/HW5LMhandout.pdf>.
[28] Hoffman JD. Numerical methods for engineers and scientists. Marcel Dekker; 2001.
[29] Loulou T, Adhikari B, Lecomte D. Estimation of concentration-dependent diffusion coefficient in drying process from the space-averaged concentration versus time with experimental data. Chem Eng Sci 2006;61(22):7185–98.
[30] Skelland AHP. Diffusional mass transfer. New York: Wiley; 1974.
[31] Ozisik MN. Finite difference methods in heat transfer. CRC; 1994.
[32] Chen Z. Finite element methods and their applications. Springer-Verlag; 2005.